Int. J. Electrochem. Sci., 16 **(2021)** Article Number: 211225, doi: 10.20964/2021.12.09

International Journal of
ELECTROCHEMICAL
SCIENCE
www.electrochemsci.org

Highly sensitive electrochemical impedance spectroscopy based sensor for *Staphylococcus aureus* detection

Peng Gu[1#], *Jing Huang*[2#], *Jiajiu Yao*[3*]

[1] General Hospital of the Yangtze River Shipping, Wuhan, Hubei, 430014, China
[2] The Attached Hospital of Northeast Teachers University, Changchun, Jilin, 134000, China
[3] Emergency Department, Tangdu Hospital, Air Force Military Medical University, Xi'an, Shaanxi 710038, China
[*]E-mail: jiajiuyao_air@sina.com

Received: 3 August 2021 / *Accepted:* 18 September 2021 / *Published:* 10 November 2021

Staphylococcus aureus is now considered one of the major pathogen of prostatitis. Its resistance to multiple drugs makes it difficult to treat, leading to a high morbidity and mortality rate. Therefore, it is imperative to establish sensitive, rapid and timely methods for the detection of *Staphylococcus aureus*. In this work, an electrochemical impedance spectroscopy sensor based on functionalized gold nanoparticles was constructed and realized for the rapid and highly sensitive analysis as well as the detection of *Staphylococcus aureus*. The experimental results demonstrated that the biosensor has a detection limit of 3×10^3 CFU/mL and a linear response range of $3 \times 10^3 – 3 \times 10^7$ CFU/mL, which means a high sensitivity. In addition, the sensor has a short detection time, simple operation and high stability, which can be used for real-time detection.

Keywords: *Staphylococcus aureus*; EIS; Biosensor; AuNPs; Prostatitis

1. INTRODUCTION

Prostatitis has long been believed to be associated with age, low immune function, and a weakened resistance of the body to disease. For some patients, the genitourinary tract has its own pathological basis, which can trigger infection by disrupting the natural defense mechanisms [1]. It was previously assumed that the most common non-specific bacterial infections of the male urogenital system were caused by gram-negative bacilli from the digestive tract, such as *Escherichia coli*, *Proteus mirabilis*, and occasionally *Neisseria gonorrhoeae*. However, some studies today suggest that the main bacteria associated with prostatitis are *Staphylococcus aureus* [2–4], which is capable of producing a large number of toxins both inside and outside the cell, causing damage to biofilms through direct interaction with the host, which leads to cell death. These toxins include staphylococcal enterotoxins

(SEA, SEB, SEC, SED, SEE, SEG, SHE, and SEI), toxic shock syndrome toxin-1 (TSST-1), and leukocidin killers. They are highly infectious or toxic and resistant to high temperatures [5–7]. The toxins survive even when *Staphylococcus aureus* is killed by heat treatment [8]. Therefore, studies on the detection of *Staphylococcus aureus* are of great significance.

Plate colony counting is the traditional detection method of *Staphylococcus aureus*, counting the number of bacteria contained in the sample [9,10]. Its basic principle is that after the sample to be tested is properly diluted, an appropriate amount of dilution is taken and spread on an agar culture dish, and under a certain temperature and a certain time of incubation, each cell can grow into a single colony visible to the naked eye [11]. According to the inoculum amount and dilution times, the number of bacteria contained in the sample is determined. Despite good accuracy and high sensitivity, this method is time-consuming with high labor cost, which is not suitable for large-scale and real-time detection of *Staphylococcus aureus* in samples. Immunological methods for the detection of *Staphylococcus aureus* include immunodiffusion, radioimmunoassay, immunoblotting, reverse passive latex agglutination assay and enzyme-linked immunosorbent assay [12], among which the immunodiffusion method was the first to be applied and was divided into one-way immunodiffusion and two-way immunodiffusion methods. However, both methods have disadvantages such as low sensitivity and the need for sample enrichment, thus they have not been promoted [13]. The radioimmunoassay combines the specificity of antigen-antibody reaction and the high sensitivity of isotope determination, which improves the specificity and sensitivity of detection. However, this method has radioactive contamination and is not easily promoted. The reverse passive latex agglutination assay is based on the same principle as the reverse indirect coagulation assay, but the reaction takes 16-24 h for the detection [14].

Biosensor is a combination of a substance to be measured with a biosensitive material that allows a specific biochemical reaction to occur and converts the resulting chemical signal into an optical or electrical signal [15]. Optical, electrochemical and piezoelectric biosensors are mainly applied in the detection of pathogenic bacteria. Electrochemical biosensors are the devices that consist of a biological identification element and a signal element to detect the target analyte [16]. The recognition element is generally a biological material, and the signal transducer is mainly an electrode. There are three major types of electrochemical biosensors, including resistance type, potential type and current type. The first one is used for bacterial detection and the latter two are commonly used for virus detection [17]. Electrochemical immunosensors are based on the specificity of antigen-antibody binding, which shows a linear relationship between the electrical signal and the concentration of the substance within a certain range, thus they can be well adopted to determine and analyze the target [18–20]. The specific binding of antigens and antibodies determines a number of positive properties of electrochemical immunosensors, including high sensitivity, being not interfered by other substances in the solution, and the reduction of the lower limit of detection. Therefore, electrochemical immunosensors, as a branch of immunosensors, are often applied in the detection of pathogens and can obtain favorable results [21–23].

In recent years, the emergence of nanotechnology has opened new research area for electrochemical biosensors. Nanomaterials have unique catalytic properties, photoelectrochemical properties, and excellent biocompatibility, and are therefore widely applied in electrochemical biosensors. For example, carbon-based nanomaterials, noble metal nanoparticles and nanocomplexes

have become increasingly popular and are used for highly loaded binding labels and amplifying electrochemical signals [24–29]. Nanomaterials, as immobilization carriers for biomolecules, have flexible pores adapted to the size of the biomolecule guest, and can also protect the immobilized biomolecules from environmental changes. The excellent properties of nanomaterials can immobilize biomolecules on the electrode surface.

AuNPs are capable of rapid and direct electron transfer between a wide range of electroactive substances and electrode materials. The light scattering properties of the local electromagnetic field and the great enhancement capabilities allow AuNPs to be applied as signal amplification tags for a variety of biosensors [30]. Their analytical performance is improved compared with other biosensor designs. In this work, an electrochemical impedance spectroscopy sensor based on functionalized gold nanoparticles was constructed and realized for the rapid and highly sensitive analysis and detection of *Staphylococcus aureus*. When *Staphylococcus aureus* reacts specifically with antibodies, it can act as a barrier to the electron transfer on the electrode surface, which is manifested by the increase of electron transfer resistance with the concentration of *Staphylococcus aureus* [31]. The prepared electrode was characterized to facilitate the understanding of the state and nature of the electrode modification layer, as well as the reaction principle of the electrode. The result shows that sensor has a high sensitivity, specificity and reproducibility for the detection of *Staphylococcus aureus*.

2. EXPERIMENTAL

2.1. Materials and instruments

Tetrachloroauric acid ($HAuCl_4$-$3H_2O$), sodium borohydride ($NaBH_4$), silver nitrate ($AgNO_3$), ascorbic acid, sodium chloride (NaCl), potassium chloride (KCl), disodium hydrogen phosphate (Na_2HPO_4), and sodium dihydrogen phosphate (NaH_2PO_4) were purchased from Shanghai Sinopharm Group Chemical Reagent Co. Polydiallyldimethylammonium chloride (PDDA, MW 200000~3500000, 20 wt %), polystyrene sodium sulfonate (PSS, MW 70000), bovine serum albumin (BSA) and cetyltrimethylammonium bromide (CTAB) were purchased from Sigma Corporation (St. Louis, MO, USA). *Staphylococcus aureus* antibody was purchased from Abcam Inc (Cambridge, UK). The CHI660D electrochemical workstation (Shanghai Chenhua Instruments Co., Ltd.) was adopted for all electrochemical experiments. Phosphate-buffered saline (PBS) applied in this work is a buffer solution commonly used in biological research and is a water-based salt solution containing disodium hydrogen phosphate, sodium chloride and potassium dihydrogen phosphate. The buffer can help to maintain a constant pH. The osmolarity and ion concentrations of the solutions match those of the human body. 1 M KCl containing 5 mM $K^3[Fe(CN)^6]^{3-/4-}$ and 0.1 M PBS were adopted for electrochemical impedance spectrum (EIS) and cyclic voltammetry (CV) analysis. A pHS-3E meter (Shanghai Youke Instrument Co., Ltd.) was used for pH detection. Scanning electron microscopy (SEM) was performed on a FEI-Sirion 200 field emission scanning electron microscope.

2.2. Preparation of AuNPs

1 mL of CTAB (0.2 M) and 1 mL of $HAuCl_4$-$3H_2O$ (0.5 mM) aqueous solution were stirred well at 25°C. The final mixture was slowly changed to brownish yellow. Afterwards, 0.12 mL of ice-cold $NaBH_4$ (0.01 M) solution was added and the resulting mixture slowly turned brownish yellow. At the same temperature of 25°C, 50 mL of $HAuCl_4$-$3H_2O$ (0.001 M), 50 mL of CTAB (0.2 M) and 2.5 mL of $AgNO_3$ (5 mM) were slowly mixed in water. 650 µL of ascorbic acid (50 mM) was added and the color of the resulting solution slowly faded. Finally, 120 µL of gold seed solution was added to the growth solution and mixed slowly at 27°C for 10 min, and the color of the solution gradually changed to dark blue. The final solution obtained by this process was AuNPs.

2.3. Preparation of electrochemical impedance spectroscopy sensor

The ITO electrodes were first cleaned by ultrasonication with acetone and anhydrous ethanol for 10 min each time, after which the ITO was placed in 1 M HCl for 10 min, removed and rinsed with deionized water. The ITO was placed in a 1:1:5 (v/v) H_2O_2/NH_4OH/H_2O solution at 70°C for 1 h. After rinsing with deionized water 3 to 5 times, the electrodes were dried in a hot air stream at 80 °C for 4 h to ensure a clean and dry surface. 20 µL of aqueous PDDA (1 mg/mL PDDA) and 20 µL of aqueous PSS (1 mg/mL) were stepwise dropped on to ITO for 30 min (denoted as ITO/PDDA/PSS). 20 µL of the prepared AuNPs solution was applied to the previously treated electrode for 1 h (denoted as ITO/PDDA/PSS/Au). 15 µL of 100 µg/mL anti- *Staphylococcus aureus* antibody was added to the electrode for 1 h at 4°C in the refrigerator, and the non-functionalized anti-*Staphylococcus aureus* was gently washed with phosphate buffer solution (denoted as ITO/PDDA/PSS/Au/Ab). A 20 µL solution of BSA (1 mg/mL) was coated for 1 h to close the non-specific reaction site (denoted as ITO/PDDA/PSS/Au/Ab/BSA). Subsequently, 20 µL of gradient-diluted *Staphylococcus aureus* liquid was added to the electrode (denoted as ITO/PDDA/PSS/Au/Ab/BSA/S). The reaction was incubated for 1 h, and the unrecognized bound *Staphylococcus aureus* was gently washed with phosphate buffer solution. The construction and detection process of the impedance spectroscopy sensor is shown in Figure 1.

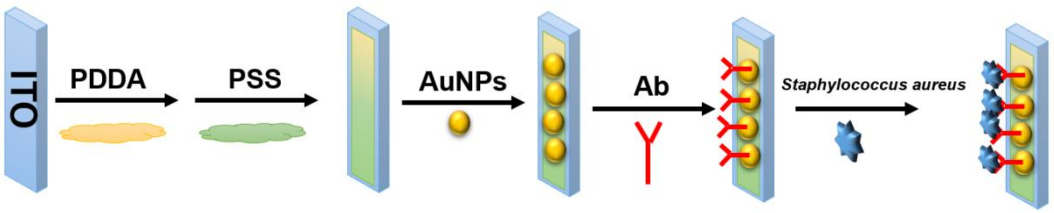

Figure 1. Schematic representation of label-free impedance spectroscopy sensor.

3. RESULTS AND DISCUSSION

The process of functionalization of AuNPs on the electrode surface is based on the electrostatic interaction between polyelectrolytes and nanoparticles with the process of layer-by-layer assembly of polyelectrolytes, which has been applied in the process of functionalization of various nanomaterials [32]. Figure 2 shows the UV as well as SEM images of AuNPs solutions. It can be seen that the synthesized AuNPs are around 80 nm in length and are uniform in size and distribution. The UV-visible spectrograms present that the absorption peaks at wavelengths around 550 nm correspond to a small amount of Au nanoparticles and those around 650 nm correspond to Au nanorods, which is consistent with literature reports [33].

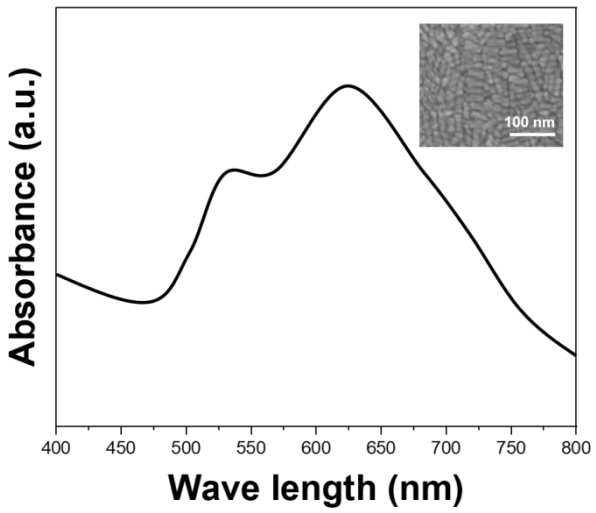

Figure 2. UV-vis spectrum and SEM image of AuNPs.

The reversible voltammetric curve of ITO electrodes is determined by the Bulter-volmer equation. Figure 3 reveals that the redox current of the ITO electrode decreases after the silanization of the electrode surface, the reason for which is that silane, antibodies, and different concentrations of *Staphylococcus aureus* are coated on the surface of the electrode. As the thickness of the film increases, the redox effect on $Fe(CN)_6^{3-/4-}$ diffusion to the surface of the electrode gradually increases the ease of charge transfer reaction. In the cyclic voltammetric scan of the $Fe(CN)_6^{3-/4-}$ reversible system, the difference between the peak anode scan potential E_{pa} and the peak cathode scan potential E_{pc} (ΔE_p) can be adopted to detect whether the electrode reaction is a Nernst reaction [34]. When the ΔE_p of an electrode reaction is close to 59/ mV (n is the number of electrons transferred), it can be determined that the reaction is a Nernst reaction. From curve a, it can be noted that ΔE_p is close to 59 mV. By comparing curve b and curve c, it can be seen that the active site of unbound antibody is blocked by the addition of BSA solution [35], which compensates for some of the unbound sites in the membrane layer, resulting in a decrease in the redox current and an increase in the distance of the redox peak. Curve d indicates that the redox current is further reduced by the addition of the target antigen. Meanwhile, the distance of the redox peak increases further, which means that the bacteriophage has a significant effect on the

blockage of charge transfer by redox. ΔE_p increases with the thickness of the biofilm on the electrode surface, indicating that the reversibility of the electrode reaction was decreasing.

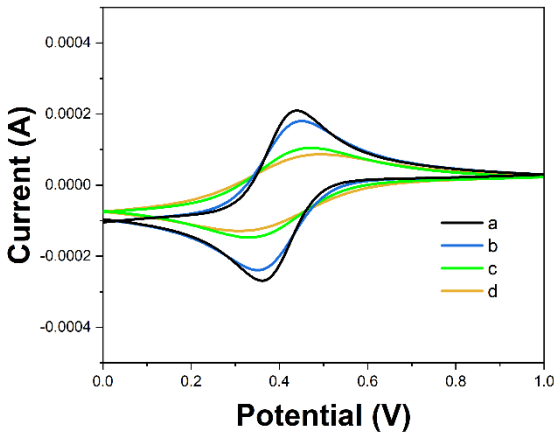

Figure 3. Cyclic voltammograms for (a) ITO/PDDA/PSS/Au, (b) ITO/PDDA/PSS/Au/Ab, (c) ITO/PDDA/PSS/Au/Ab/BSA and (d) ITO/PDDA/PSS/Au/Ab/BSA/S in 0.01 M PBS (pH 7.4) containing 5.0 mM $[Fe(CN)_6]^{3-/4-}$ (scan rate: 50 mV/s).

Electrochemical impedance spectroscopy is performed near the electrode equilibrium potential, which has a low impact on the biofilm and allows for the fitting of an equivalent circuit to the system [36]. In an electrochemical cell containing a redox probe, the equivalent circuit can be represented in Figure 4 in the presence of both electrochemical polarization and concentration polarization [37]. The resistance of the electrolyte is R_S, the double layer generated by the charge at the interface is C_d, and the impedance resulted from charge migration during redox reactions is R_{ct}. When performing polarization, it is also necessary to consider the impedance containing new resistance and capacitive components (Warburg impedance). Z_W, R_S and Z_W represent the impedance of the electrolyte solution and the diffusion characteristics of the redox probe in solution, respectively, which are not influenced by the electrochemical reactions on the electrode surface. The other two parameters, C_d and R_{ct}, are mainly determined by the dielectric properties and insulating properties of the electrolyte/electrode surface [38]. The electrochemical impedance of an electrode consists of a real part and an imaginary part, and the Nyquist diagram, which plots the imaginary part of the impedance against the real part of the impedance, is the most common form of impedance data representation [39] and is particularly suitable for representing the magnitude of impedance changes in a system.

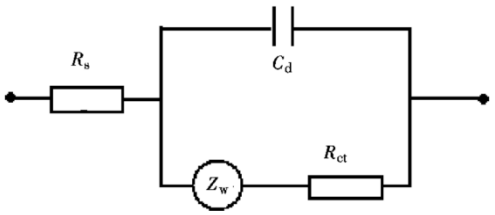

Figure 4. Equivalent circuit diagram for electrochemical detection.

As shown in Figure 5, the R_{et} of the bare electrode ITO (line a) is 107 Ω. The PDDA, being positively charged and not conducting itself, hinders the electron transfer, as shown by the increase in R_{et} to 477.6 Ω (line b). PSS has a negative charge and the interaction between positive and negative charges fixes the PSS on the electrode surface. Since the homogeneous repulsion has a significant hindering effect on the electron transfer, the resistance R_{et} of ITO/PDDA/PSS increases significantly to 1566.5 Ω (line c). The impedance of ITO/PDDA/PSS/Au decreases significantly to 337.2 Ω (line d) compared with the previous two. The reasons for this phenomenon are: 1) AuNPs are inherently conductive and contributive to electron transfer, and 2) the positive charge of AuNPs and the negatively charged $[Fe(CN)_6]^{3-/4-}$ in solution contribute to electron transfer due to positive and negative charge interactions. The attachment of antibodies and *Staphylococcus aureus* that are both biological macromolecules, further hinders the electrons from the solution from reaching the electrode surface. Thus the further increases of electron transfer resistance were 586.8 Ω (line e) and 915.0 Ω (line f), respectively. The above experiments have confirmed the success of the electrode surface modification, and also detected the value of the change in resistance due to the immune reaction [40].

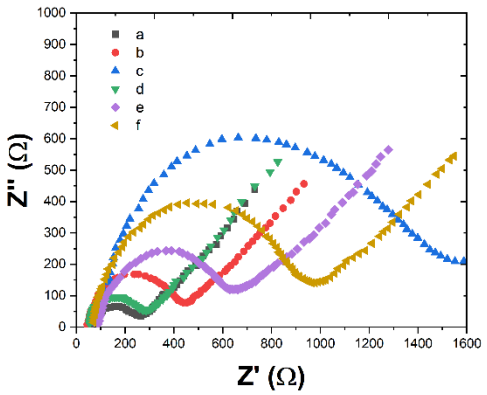

Figure 5. Nyquist plots of (a) ITO. (b) ITO/PDDA, (c) ITO/PDDA/PSS, (d) ITO/PDDA/PSS/Au, (e) ITO/PDDA/PSS/Au/BAS and (f) ITO/PDDA/PSS/Au/BAS/S in 0.01 M PBS (pH 7.4) containing 5.0 mM $[Fe(CN)_6]^{3-/4-}$.

The results of the above experiments demonstrate that electrochemical impedance spectroscopy is a good interfacial characterization technique for the qualitative detection of *Staphylococcus aureus*. In this work, the specific recognition of antigen-antibody is the principle on which the sensor works. The immunocomplex (i.e., the antigen–antibody complex) is directly determined by the measuring of the physical changes induced by the formation of the complex. In this case, the EIS change during the different concentrations of *Staphylococcus aureus* has been used as signal [41]. Moreover, we have tried to quantify *Staphylococcus aureus* by applying electrochemical impedance spectroscopy biosensors. The ITO/PDDA/PSS/Au/BAS was incubated with different concentrations of *Staphylococcus aureus* to allow the sufficient reaction of the antigen and antibody, which was subsequently placed in the electrochemical detection cell for electrochemical impedance spectroscopy. The results are shown in Figure 6. It is clear that the measured charge transfer impedance increases with the concentration of the

Staphylococcus aureus. The specific impedance values are shown in Table 1. The sensor has a good linear relationship in the detection range. The response equation for the rate of change of resistance and concentration is:

R_{ct} =123.02 LogC – 260.26

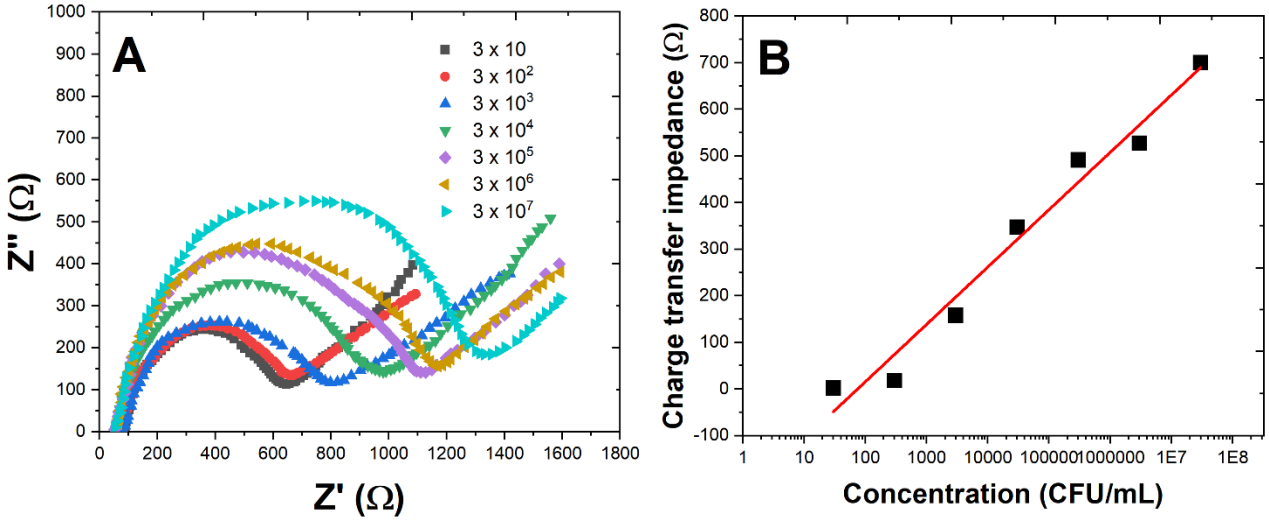

Figure 6. (A) The electrochemical impedance spectra of *Staphylococcus aureus* bound to ITO/PDDA/PSS/Au/BAS at different concentrations. a to f represent the *Staphylococcus aureus* concentration (CFU/mL): 3 × 10; 3 × 10^2; 3 × 10^3; 3 × 10^4; 3 × 10^5; 3 × 10^6, 3 × 10^7 in 0.01 M PBS (pH 7.4) containing 5.0 mM $[Fe(CN)_6]^{3-/4-}$. (B) Calibration curves of the bacterial concentration vs. charge transfer impedance.

Table 1. Bacterial concentration vs. charge transfer impedance relationship.

Concentration (CFU/mL)	3 × 10	3 × 10^2	3 × 10^3	3 × 10^4	3 × 10^5	3 × 10^6	33 × 10^7
Charge transfer impedance (Ω)	2.41	18.21	157.7	346.69	491.19	527.39	699.97

For the purpose of testing the selectivity of the sensor, five other species were selected as comparators: *E. coli, S. typhimurium, B. pumilus, K. pneumoniae* and *B. subtilis*. The ΔR_{et} were measured by adding different strains of the same concentration dropwise on the electrode surface as shown in Figure 7. The value of ΔR_{et} was less than 300 Ω as the five species were added dropwise, while the value of ΔR_{et} for *Staphylococcus aureus* was 911.4 Ω. The major reason for such a significant change is the specificity of the antibody for antigen recognition. The results again indicate that the immunosensor is feasible for the detection of *Staphylococcus aureus*.

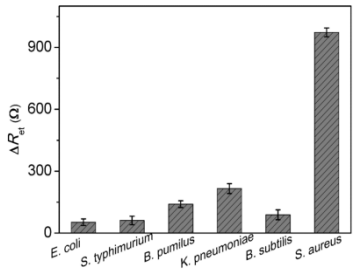

Figure 7. Specificity investigation of the proposed sensors towards *E. coli, S. typhimurium, B. pumilus, K. pneumoniae, B. subtilis* and *S. aureus*.

The experiments also examined the detection of this sensor on real samples. A serum spiked with *Staphylococcus aureus* was selected as the sample for the assay. 1 μL of serum was taken and diluted to 1 mL of sample by adding PBS (pH 7.4). The sample was divided into four portions and spiked with different concentrations of *Staphylococcus aureus.* The sensor was adopted to test each of the above treated samples, and the procedure was repeated three times with the results shown in Table 2. The relative standard deviations of the immunosensor were in the range of 1.75%-2.75%, indicating that the immunosensor is accurate and can be applied to the actual samples.

Table 2. Determination of *Staphylococcus aureus* in serum samples by using the proposed sensor and plate count method.

Sample	*Staphylococcus aureus* concentration (CFU/mL)				RSD (%)
	Blank	Added	Found	Plate count	
1	/	4.00×10^2	4.07×10^2	4.03×10^2	1.75
2	/	4.00×10^3	4.10×10^3	4.19×10^3	2.50
3	/	4.00×10^4	3.89×10^4	3.84×10^4	2.75

4. CONCLUSION

In this work, a new electrochemical sensor for *Staphylococcus aureus* detection was prepared based on electrochemical impedance spectroscopy with AuNPs immobilized on the surface of silanized ITO electrodes. The preliminary detection of *Staphylococcus aureus* was achieved with electrochemical impedance spectroscopy. The experimental results demonstrate that the biosensor has a detection limit of 3×10^3 CFU/mL and a linear response range of 3×10^3 - 3×10^7 CFU/mL, which means a high sensitivity. In addition, the sensor has a short detection time, simple operation and high stability, which can be applied in real-time detection.

References

1. Y. Wu, H. Jiang, M. Tan, X. Lu, *The Prostate*, 80 (2020) 577–587.

2. A.V. Johri, P. Johri, N. Hoyle, L. Pipia, L. Nadareishvili, D. Nizharadze, *Front. Pharmacol.*, 12 (2021) 1424.
3. N.M. Ibrahim, *Eur. J. Mol. Clin. Med.*, 8 (2021) 1781–1789.
4. H. Karimi-Maleh, F. Karimi, L. Fu, A.L. Sanati, M. Alizadeh, C. Karaman, Y. Orooji, *J. Hazard. Mater.*, 423 (2022) 127058.
5. S.S. Boswihi, E.E. Udo, *Curr. Med. Res. Pract.*, 8 (2018) 18–24.
6. R. Astley, F.C. Miller, M.H. Mursalin, P.S. Coburn, M.C. Callegan, *Toxins*, 11 (2019) 356.
7. D. Oliveira, A. Borges, M. Simões, *Toxins*, 10 (2018) 252.
8. M.J. Anderson, E. Schaaf, L.M. Breshears, H.W. Wallis, J.R. Johnson, C. Tkaczyk, B.R. Sellman, J. Sun, M.L. Peterson, *Toxins*, 10 (2018) 157.
9. G. Loss, P.M. Simões, F. Valour, M.F. Cortês, L. Gonzaga, M. Bergot, S. Trouillet-Assant, J. Josse, A. Diot, E. Ricci, *Front. Cell. Infect. Microbiol.*, 9 (2019) 363.
10. N. Minh Dat, V.N.P. Linh, L.A. Huy, N.T. Huong, T.H. Tu, N.T.L. Phuong, H.M. Nam, M. Thanh Phong, N.H. Hieu, *Mater. Technol.*, 34 (2019) 369–375.
11. T.W.F. Lung, I.R. Monk, K.P. Acker, A. Mu, N. Wang, S.A. Riquelme, S. Pires, L.P. Noguera, F. Dach, S.J. Gabryszewski, *Nat. Microbiol.*, 5 (2020) 141–153.
12. A. Fetsch, S. Johler, *Curr. Clin. Microbiol. Rep.*, 5 (2018) 88–96.
13. A. Nouri, H. Ahari, D. Shahbazzadeh, *Int. J. Biol. Macromol.*, 107 (2018) 1732–1737.
14. A.T. Nguyen, S.M. Tallent, *J. AOAC Int.*, 101 (2018) 1127–1134.
15. M. Rubab, H.M. Shahbaz, A.N. Olaimat, D.-H. Oh, *Biosens. Bioelectron.*, 105 (2018) 49–57.
16. R. Cai, Z. Zhang, H. Chen, Y. Tian, N. Zhou, *Sens. Actuators B Chem.*, 326 (2021) 128842.
17. L. Xu, W. Liang, Y. Wen, L. Wang, X. Yang, S. Ren, N. Jia, X. Zuo, G. Liu, *Biosens. Bioelectron.*, 99 (2018) 424–430.
18. Y. Wang, W. Yan, S. Fu, S. Hu, Y. Wang, J. Xu, C. Ye, *Front. Microbiol.*, 9 (2018) 907.
19. H. Karimi-Maleh, Y. Orooji, F. Karimi, M. Alizadeh, M. Baghayeri, J. Rouhi, S. Tajik, H. Beitollahi, S. Agarwal, V.K. Gupta, *Biosens. Bioelectron.* (2021) 113252.
20. R. Duan, X. Fang, D. Wang, *Front. Chem.*, 9 (2021) 361.
21. C. Li, F. Sun, *Front. Chem.*, 9 (2021) 409.
22. W. Li, W. Luo, M. Li, L. Chen, L. Chen, H. Guan, M. Yu, *Front. Chem.*, 9 (2021) 610.
23. J. Liu, T. Yang, J. Xu, Y. Sun, *Front. Chem.*, 9 (2021) 488.
24. S. Eissa, M. Zourob, *Analyst*, 145 (2020) 4606–4614.
25. J. Zhou, R. Fu, H. Liu, Y. Liu, Y. Wang, B. Jiao, Y. He, H. Tang, *J. Hazard. Mater.* (2021) 126223.
26. L. Fu, K. Xie, A. Wang, F. Lyu, J. Ge, L. Zhang, H. Zhang, W. Su, Y.-L. Hou, C. Zhou, C. Wang, S. Ruan, *Anal. Chim. Acta*, 1081 (2019) 51–58.
27. J. Zhou, Y. Zheng, J. Zhang, H. Karimi-Maleh, Y. Xu, Q. Zhou, L. Fu, W. Wu, *Anal. Lett.*, 53 (2020) 2517–2528.
28. L. Fu, W. Su, F. Chen, S. Zhao, H. Zhang, H. Karimi-Maleh, A. Yu, J. Yu, C.-T. Lin, *Bioelectrochemistry* (2021) 107829.
29. Y. Xu, Y. Lu, P. Zhang, Y. Wang, Y. Zheng, L. Fu, H. Zhang, C.-T. Lin, A. Yu, *Bioelectrochemistry*, 133 (2020) 107455.
30. V.Q. Khue, T.Q. Huy, V.N. Phan, A. Tuan-Le, D.T.T. Le, M. Tonezzer, N.T.H. Hanh, *Mater. Chem. Phys.*, 255 (2020) 123562.
31. X. Yang, L. Zhang, X. Jiang, *Nano Res.*, 11 (2018) 6237–6243.
32. R. Shahbazi, M. Salouti, B. Amini, A. Jalilvand, E. Naderlou, A. Amini, A. Shams, *Mol. Cell. Probes*, 41 (2018) 8–13.
33. S. Yao, J. Li, B. Pang, X. Wang, Y. Shi, X. Song, K. Xu, J. Wang, C. Zhao, *Microchim. Acta*, 187 (2020) 1–8.
34. J. Muñoz, R. Montes, M. Baeza, *TrAC Trends Anal. Chem.*, 97 (2017) 201–215.
35. J.S. Park, H.J. Kim, J.-H. Lee, J.H. Park, J. Kim, K.S. Hwang, B.C. Lee, *Sensors*, 18 (2018) 426.

36. R. Maallah, A. Moutcine, C. Laghlimi, M. Smaini, A. Chtaini, *Sens. Bio-Sens. Res.*, 24 (2019) 100279.
37. A. Khoshroo, L. Hosseinzadeh, A. Sobhani-Nasab, M. Rahimi-Nasrabadi, F. Ahmadi, *Microchem. J.*, 145 (2019) 1185–1190.
38. R. Khadka, N. Aydemir, C. Carraher, C. Hamiaux, D. Colbert, J. Cheema, J. Malmström, A. Kralicek, J. Travas-Sejdic, *Biosens. Bioelectron.*, 126 (2019) 207–213.
39. S. Dhillon, R. Kant, *J. Chem. Sci.*, 129 (2017) 1277–1292.
40. Z. Jiang, J. Yao, L. Wang, H. Wu, J. Huang, T. Zhao, M. Takei, *IEEE Sens. J.*, 19 (2019) 5979–5987.
41. F. Mollarasouli, S. Kurbanoglu, S.A. Ozkan, *Biosensors*, 9 (2019) 86.